ASCE Author Proofs

Important Notice to Authors

Attached is a PDF proof of your forthcoming article in **International Journal of Geomechanics**. The manuscript ID number is **GMENG-5372**.

No further publication processing will occur until we receive your response to this proof. Please return any corrections within 48 hours of receiving the download email. Your paper will be published in its final form upon receipt of these corrections. You will have no further opportunities to review your proof or to request changes after this stage.

Information and Instructions

- The graphics in your proof have been down-sampled to produce a more manageable file size and generally represent the online presentation. Higher resolution versions will appear in print.
- Proofread your article carefully, as responsibility for detecting errors lies with the author.
- Mark or cite all corrections on your proof copy only.
- Corrections should be completed within 48 hours after receipt of this message.
- If no errors are detected, **you are still required to log in, make note in the proof, and finalize the article to indicate that it is okay** to be published as is.
- You will receive a message confirming receipt of your corrections within 48 hours.

Questions and Comments to Address

The red numbers in the margins correspond to queries listed on the last page of your proof. Please address each of these queries when responding with your proof corrections.

Return your Proof Corrections

- Web: If you accessed this proof online, follow the instructions on the Web page to submit corrections.
- E-mail: Send corrections to ascejournals@novatechset.com. Include the manuscript ID GMENG-5372 in the subject line. Please do not provide a revised manuscript.

Please annotate and complete your proof review within 48 hours. Should this not be possible or should you encounter any problems or have further questions, please contact the Journal Production Manager at ascejournals@novatechset.com and include GMENG-5372 in the subject line.

ASCE Open Access

Authors may choose to publish their papers through ASCE Open Access, making the paper freely available to all readers via the ASCE Library website. ASCE Open Access papers will be published under the Creative Commons-Attribution Only (CC-BY) License. The fee for this service is $2,000, and must be paid prior to publication. If you indicate Yes, you will receive a follow-up message with payment instructions. If you indicate No, your paper will be published in the typical subscribed-access section of the Journal.

Selecting Yes does not commit you to publishing your article as Open Access. You will have the option to cancel the Open Access process later. If you are unsure, we recommend selecting Yes. If you select No now, your paper will be published online shortly after your proof corrections are received, and you will no longer have the ability to publish your article as Open Access.

Color Figures

Figures containing color will appear in color in the online journal. All figures will be grayscale in the printed journal unless you have agreed to pay the color figure surcharge and the relevant figure caption indicates “(Color)”. For figures that will be in color online but grayscale in print, please ensure that the text and captions do not describe the figures using colors.

If you have indicated that you will be printing color figures in color, you will receive a notification with a link to the payment system. Until payment is received or color printing is canceled, your article will not be published.

Reprints

If you would like to order reprints of your article, please visit https://www.asce.org/reprints.

ASCE

Steady-State Groundwater in Mechanical Stabilized Earth Walls of Various Dimensions with Geocomposite Back Drain Installation

Hai La Duong[1]; Avirut Chinkulkijniwat[2]; Suksun Horpibulsuk, Ph.D., P.E.[3]; Thien Do Quang[4]; and Teerasak Yaowarat, Ph.D.[5]

Abstract: Recently, considerable risks to the internal instability of mechanically stabilized earth (MSE) walls have been encountered from the inadequate drainage capacity of some backfill under extremely heavy rainfall. Due to its high drainage capacity, geocomposite is regarded as an appropriate material for drainage purposes in many geotechnical structures, including MSE walls. However, the installation of a geocomposite drain produces hydrologically complex boundary conditions, and unsaturated flow through the MSE wall becomes more complicated. This article reports a series of numerical simulations conducted to investigate the influences of MSE wall dimensions and drainage capacity on seepage responses inside the protected zone of the wall. The results indicated that the distance from the upstream water source to the drainage face (L) contributes most to the level of the phreatic surface inside the protected (reinforced) zone. Furthermore, a relationship existed between the permeability of the soil on the upstream side and the lowering of the phreatic surface due to increased geonet transmissivity. Results reported in this study might reinforce understanding of complex flow behaviors in MSE walls with back drain installation.
DOI: 10.1061/(ASCE)GM.1943-5622.0001946.

Author keywords: MSE wall; Geocomposite; Steady-state flow; Shape parameters; Phreatic level; Geonet transmissivity.

Introduction

Mechanically stabilized earth (MSE) walls have been widely used in cut-and-fill works for highway construction through mountainous areas. Although MSE walls are very effective for cut-and-fill works in sloping ground, several MSE wall failures during heavy rainfall have been reported (Yoo and Jung 2006; Vahedifard et al. 2017). Internal instability is one of the most often reported failure modes in MSE walls (Koerner and Koerner 2011, 2013; Thuo et al. 2015; Robinson et al. 2017; Koerner and Koerner 2018). Heavy rainfall might cause an increment of water content and phreatic level in MSE walls and, hence, the drop of soil suction. Based on the extended Mohr–Coulomb criterion proposed by Fredlund et al. (1978), cohesive strength is divided into two components: (1) cohesion c'; and (2) apparent cohesion due to suction. Escario and Sáez (1986), among others, reported from their test results a nonlinear drop of the apparent cohesion due to the increment of water content, and hence suction drop. Iryo and Rowe (2004) and Thuo et al. (2015) reported serious reductions in shear strength of the soil in the reinforced zone due to extreme precipitation. Koerner and Koerner (2018) reported that 41% of all internal failures were caused by the poor performance of the drainage system. Other than internal stability, Zhang et al. (2016) reported the influence of water content on the external stability of retaining walls. In order to avoid high water content in MSE walls, the drainage system must have a high enough capacity to drain sufficient water in extreme conditions.

To combine high drainage capacity and ease of installation, drainage systems installed in many geostructures, including MSE walls, have frequently used a geocomposite comprising a geonet core with a large flow channel sandwiched by a nonwoven geotextile (Zornberg et al. 1995; McKean and Inouye 2001; Koerner and Koerner 2011, 2013, 2015). This type of geocomposite system installed as a back drain for an MSE wall is the focus of this study. Although geocomposite drains in MSE walls have been spotlighted in various reports, most of these works focused on aspects of material properties, particularly the influence of factors affecting geonet transmissivity. Dickinson et al. (2010) determined the relationship between geonet transmissivity and geonet thickness. Giroud and Kavazanjian (2014) and Yarahmadi et al. (2017) studied the reduction of hydraulic transmissivity due to creep deformation. Reports about the influence of geocomposite properties on seepage responses in MSE walls are limited. Chinkulkijniwat et al. (2017) concluded that the capillary barrier phenomenon plays a role in the distribution of effective saturation at the soil–geotextile interface. Bui Van et al. (2017) proposed that the outer permeability

[1]Ph.D. Scholar, School of Civil Engineering, Institute of Engineering, Suranaree Univ. of Technology, 111 University Avenue, Suranaree, Muang, Nakhon Ratchasima 30000, Thailand. Email: hailaduong9@gmail.com

[2]Professor, Center of Excellence in Civil Engineering, School of Civil Engineering, Institute of Engineering, Suranaree Univ. of Technology, 111 University Avenue, Suranaree, Muang, Nakhon Ratchasima 30000, Thailand (corresponding author). ORCID: https://orcid.org/0000-0003-4905-7991. Email: avirut@sut.ac.th

[3]Professor, School of Civil Engineering, Institute of Engineering, Suranaree Univ. of Technology, 111 University Avenue, Suranaree, Muang, Nakhon Ratchasima 30000, Thailand. Email: suksun@g.sut.ac.th

[4]Associate Professor, Hydrogeology and Engineering Geological Department, Faculty of Geography and Geology, Hue Univ. of Sciences, Nguyen Hue St., Hue City, Thua Thien Hue 49000, Vietnam. Email: dqthien@hueuni.edu.vn

[5]Post Doctoral Researcher, School of Civil Engineering, Institute of Engineering, Suranaree Univ. of Technology, 111 University Avenue, Suranaree, Muang, Nakhon Ratchasima 30000, Thailand. Email: teerasakyaowarat@gmail.com

Note. This manuscript was submitted on November 5, 2019; approved on October 14, 2020No Epub Date. Discussion period open until 0, 0; separate discussions must be submitted for individual papers. This paper is part of the ***International Journal of Geomechanics***, © ASCE, ISSN 1532-3641.

ratio, defined as a ratio of geonet permeability to permeability of upstream soil, affected the phreatic level in the protected zone. No correlation between the phreatic level in the protected zone and the permeability ratio was provided since only four simulation cases related to the outer permeability ratio were conducted in their report. This study conducted a series of numerical experiments for further elaborating the finding in Bui Van et al. (2017).

Other than geocomposite properties, the hydrological properties of the relevant soils also play an important role in seepage responses such as the distribution of water content and the location of the phreatic surface in MSE walls. A number of studies reported the effect of hydrological properties of the soil on seepage responses in MSE walls (Zornberg and Mitchell 1994; Christopher et al. 1998; Vahedifard et al. 2017; Albino et al. 2019). In mountainous terrain, where heavy rainfall could raise the upstream water level due to huge amounts of rainwater flowing from high ground toward an MSE wall (Bui Van et al. 2017), the seepage responses in the MSE wall were also governed by the relevant shape parameters. These parameters included the level of the upstream water table, the distance from the upstream water to the drainage face, the depth below the wall of the impervious rock interface, and the width and height of the protected zone. Theoretically, these shape parameters affect groundwater flow geometry and, hence, related seepage responses.

For steady-state unconfined flow in rectangular-flow systems, Clement et al. (1996) investigated the effect of the flow domain aspect ratio on the height of the seepage face, which is the difference between the phreatic surface at the exit and the downstream water level. They found that effects on the seepage face were diminished for long, shallow flow domains, while the position of the phreatic surface was relatively insensitive to downstream water level for deep flow domains. Saeedpanah et al. (2011) reported that the length of the groundwater flow path plays a more important role in the flow rate than the upstream water level does. Despite their importance to seepage responses, the relevant shape parameters are yet to be investigated thoroughly enough to comprehensively explain their influence on seepage responses in an MSE wall.

In this study, a well-calibrated numerical model, computed in the Plaxis environment and introduced by Chinkulkijniwat et al. (2017), was further elaborated with regard to the effect of scaling. To ensure the validity of the Plaxis-based model on different scales, it was established using identical shape ratios at double the size of the physical model. The calibrated model was further employed to perform a series of parametric studies focusing on the influence of the shape parameters and geonet transmissivity on seepage responses in the modeled MSE wall. Results from this study reinforces research into the influence of the dimensions of MSE walls and drainage properties on seepage responses.

Governing Equations

The equation governing transient water flow for a two-dimensional homogeneous anisotropic material within an unsaturated porous medium is given as follows:

$$k_x \frac{\partial^2 h}{\partial x^2} + k_y \frac{\partial^2 h}{\partial y^2} = \frac{\partial \theta}{\partial t} \tag{1}$$

where θ = volumetric water content, which is defined as the volume of water present in a unit volume of soil mass; h = total head; k_x and k_y = unsaturated coefficients of permeability in the $x-$ and $y-$directions; and t = time. When the variables describing the water states at a given point do not change in time, the flow is treated as steady, the time derivatives in the equations of motion are zero and Eq. (1) becomes

$$k_x \frac{\partial^2 h}{\partial x^2} + k_y \frac{\partial^2 h}{\partial y^2} = 0 \tag{2}$$

To supplement Eq. (2), constitutive equations are required, relating θ, k_x, and k_y to h. In this study, the van Genuchten (1980) model [Eq. (3*a*)] and the van Genuchten–Mualem model [Eq. (3*b*)], which is an integration of the van Genuchten model with the Mualem hypothesis (Mualem 1976), were employed to approximate the water retention curve (WRC) and permeability functions for every porous media in the MSE wall problem. These models are later named in this paper as VG and VGM models, respectively. The models gave the following equations:

$$S_e = \frac{S - S_{\text{res}}}{S_{\text{sat}} - S_{\text{res}}} = \frac{\theta - \theta_{\text{res}}}{\theta_{\text{sat}} - \theta_{\text{res}}} = [1 + (\alpha |h_p|)^n]^{-m} \tag{3a}$$

$$k_r(S_e) = S_e^{0.5}[1 - (1 - S_e^{1/m})^m]^2 \tag{3b}$$

In the aforementioned equations, S_e = effective degree of saturation; S = degree of saturation; S_{res} = residual saturation at very high values of suction; S_{sat} = maximum saturation of saturated soil; θ_{res} = residual volumetric water content; θ_{sat} = maximum volumetric water content of saturated soil; h_p = matric suction head; and k_r = relative permeability coefficient: α [m^{-1}] and n are fitting parameters that represent, respectively, the air-entry value of the soil and the rate of water extraction from the soil once the air-entry value has been exceeded: m, according to the Mualem (1976) hypothesis, is assigned the value $1 - 1/n$. Steady-state flow conditions were the focus of our study in order to quantify the final state of groundwater flow in the porous media.

Materials and Methods

Fig. 1 presents a sketch of a physical model designed to investigate responses in an MSE wall with a geocomposite installation as a back drain under a high upstream ground water level. This large-scale model was established by Chinkulkijniwat et al. (2017), who also reported the results from tests conducted with this model filled with sandy soil. Basic and hydrological properties of the studied materials, including sandy soil, lateritic soil, geotextile, and geonet, are given in Fig. 2 and Table 1. Fig. 2(a) presents the grain size distribution of the sandy soil and the lateritic soil. Since the problem in this study involves with water flow into the MSE wall, the wetting phase water retention curve (WRC) of the corresponding materials must be obtained. Fig. 2(b) presents the wetting phase WRC of sandy soil, lateritic soil, and geotextile. Nonlinear regression was conducted fit the VG model [Eq. (3*a*)] to the measured WRC. The best-fit VG model parameters of the studied materials are also given in Table 1. Although we obtained the wetting phase WRC from the previous studies (Chinkulkijniwat et al. 2017; Bui Van et al. 2017), determinations of WRC are briefly given in the following for clarification.

Different techniques were employed to obtain the curves. The wetting phase WRC of the geotextile was obtained from a capillary rise test (Lafleur et al. 2000). The wetting phase WRC of the sandy soil was obtained using the double-walled triaxial cell. Due to the difficulty of direct determination of the wetting phase WRC in the lateritic soil, the drying phase WRC of the lateritic soil was obtained using a pressure plate apparatus (ASTM D6836-02). After getting the best-fit VG model parameters for the drying phase WRC of the lateritic soil, every VG model parameter values for

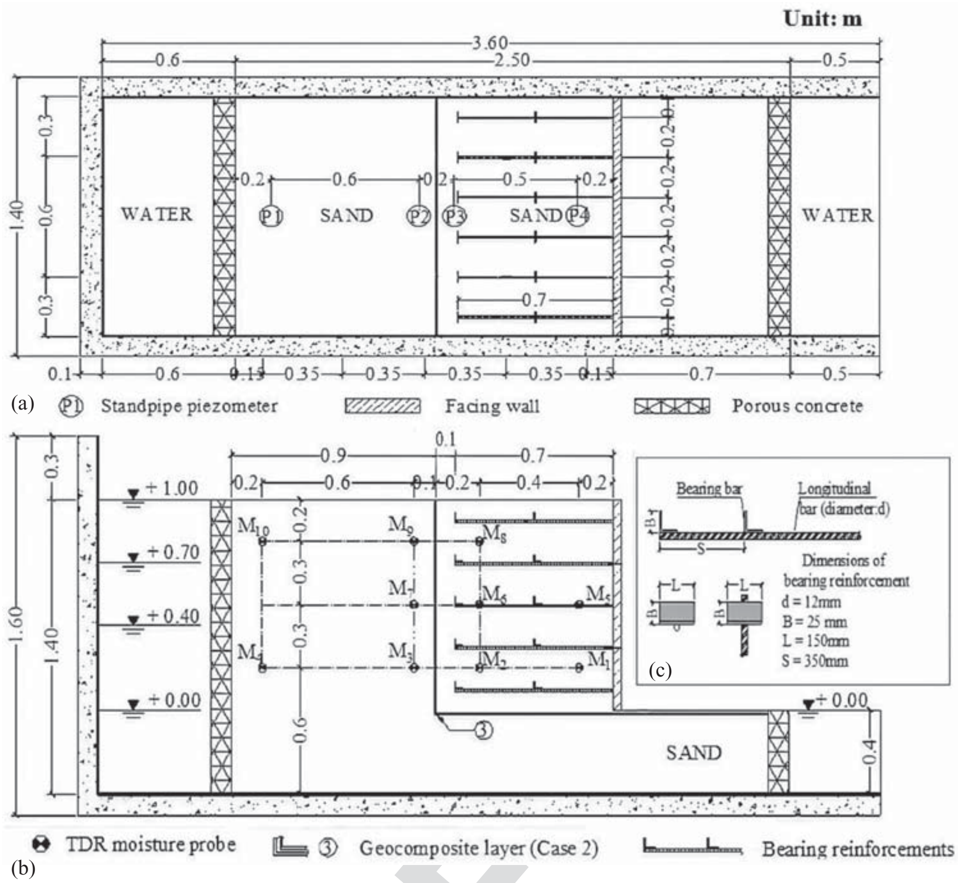

F1:1 **Fig. 1.** Physical test model and its instrumentation: (a) plan view of the model; (b) side view of the model; and (c) sketch of bearing reinforcement.
F1:2 (Adapted from Chinkulkijniwat et al. 2017.)

the drying phase WRC were assigned to the wetting phase WRC except the parameter α, which was twice as high as that for the drying phase WRC (Kool and Parker 1987). The VG model parameters of geonet was based on the physical meaning of the VG model parameters. The α parameter is related to the largest pore size, and the n parameter is related to the pore distribution. As the geonet has a very open structure, VG and VGM models with the following considerations were assigned to the geonet: (1) the geonet has a large and single pore size attribution; and (2) the geonet can be completely dried ($S_{res} = 0.0$) and completely saturated ($S_{sat} = 1.0$). With respect to the first consideration, high values of α and n reflect a large pore size and a more uniform pore size distribution, respectively. Hence, high α and n values were assigned to the geonet. According to Chinkulkijniwat et al. (2017), the geonet parameters α and n were assigned values of 600 m^{-1} and 40, respectively. These values were summarized after finding that the calculation results were not changed after assigning magnitudes of α greater than 600 m^{-1} and n greater than 40. Since it is easier to measure WRC than to measure the permeability function, estimation of the permeability function can be achieved through the model parameters extracted from the WRC of the corresponding material. Fig. 2(c) plots the permeability function of every material used in this study. At the low suction (high saturation) level, the geonet permeability is much higher than the permeability of the other studied materials. In this condition, the geonet accepts water flowing from its adjacent material and collects water to drain away at the downstream side. The geonet permeability, however, drops sharply with suction and becomes notably lower than the permeability of the other materials. At the high suction (low saturation) level, the geonet is filled with air, and hence, no water flow across the boundary between the geonet and its adjacent material.

In the remaining part of this section, model preparation, test procedure, and test results reported by Chinkulkijniwat et al. (2017) are briefly mentioned for the sake of clarification. The sandy soil, geocomposite drain, reinforcement of the wall facing, and instrumentation were carefully positioned in the model. Groundwater flow during the test was activated by the difference of water levels in upstream and downstream water tanks. The water level in the downstream tank was kept constant at a depth of 0.4 m (+0.0 m) using a control weir. The water level in the upstream tank was increased stepwise from a depth of 0.4 m (+0.0 m), to 0.8 m (+0.4 m), 1.1 m (+0.7 m), and 1.4 m (+1.0 m). Increments in water level in the upstream tank were made when the steady state was observed, which was indicated by steady water content values, detected by time domain reflectometry (TDR) probes. Fig. 3 presents time series plots of water content at M2, M6, and M8 TDR probes and distribution of water content and groundwater levels at the steady state in sandy soil for an upstream water level of +0.4, +0.7, and +1.0 m. At any height of upstream water, the groundwater level decreased through the wall face and dropped drastically in the protected zone (or reinforced zone). The water content values in the protected zone were also much lower than that in the outside zone. These measurements showed that the installation of high permeable geocomposite could prevent water flow to the protected zone effectively.

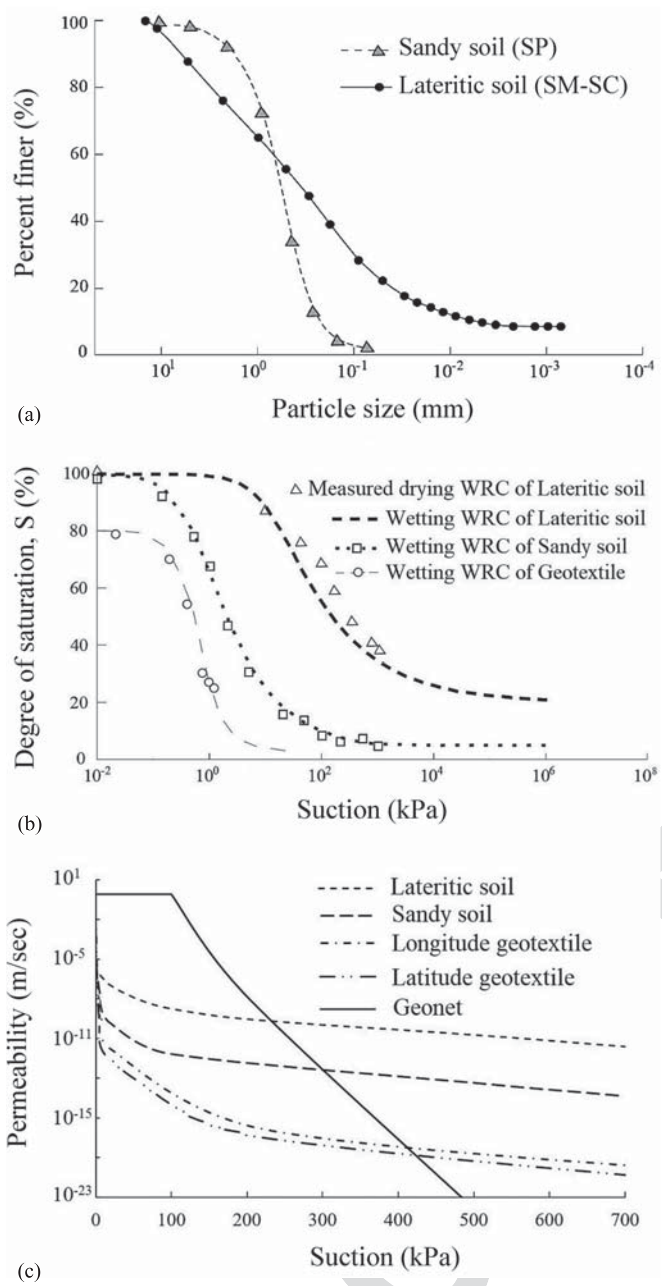

Fig. 2. (a) Grain size distribution of studied sandy soil, geotextile, and lateritic soil utilized in this study; (b) WRC of studied sandy soil, geotextile, and lateritic soil utilized in this study; and (c) permeability function of studied sandy soil, geonet, geotextile, and lateritic soil utilized in this study. (Adapted from Bui Van et al. 2017.)

Numerical Simulations

A series of numerical experiments were conducted using the finite-element code Plaxis. Fig. 4 depicts the discretized finite-element mesh for the MSE wall model and the shape parameters investigated in this study. The shape parameters included the height of the wall (H), the width of the protected zone (W), the distance from the upstream water source to the drainage face (L), and the distance from the wall base to the impervious boundary (D). The *groundwater flow only* mode was selected for the Plaxis calculations. Fifteen-node triangles were assigned to the generated models, and a fine mesh with an average element size of 0.05 m was selected. Since the hydrological related properties, including permeability and VG parameters, had to assigned to the geotextile and geonet, the geotextile and geonet in this study were prescribed as soil materials having own hydrological related properties. Finer meshes of 15-node triangle were also assigned to the geotextile and the geonet. Dirichlet boundary conditions with prescribed pressures were imposed on the left, right, and upper boundaries of the model, and the bottom boundary of the model was defined as impermeable. The left and right boundaries were assigned hydrostatic pressure, whereas the upper boundary was assigned atmospheric pressure. Groundwater flow was simulated by applying hydrostatic pressure according to the upstream water level equal to any desired height. Time steps were automatically assigned by the software. At each time step, the nonlinear differential equation [Eq. (2)] was solved iteratively using a modified Newton–Raphson model. In each iteration, the increment of the groundwater head was calculated from the imbalance in the nodal discharge and added to the active head. This process continued until the norm of the imbalanced vector—that is, the error in the nodal discharge—was smaller than that of the error tolerance of 0.01 (or 1%).

For calibration purposes, the model was designed to replicate the experimental studies mentioned previously. This model incorporated sandy soil, structural components (reinforced bar and acrylic facing), and drainage components (geotextile and geonet). The seepage characters of the relevant materials were described using Eqs. (2) and (3). To ensure the validity of the Plaxis-based model on different scales, the Plaxis-based model was established to keep identical shape ratios at double the size of the physical model: $H = 2.0$ m, $H_w = 2.0$ m, $W = 1.6$ m, and $D = 0.8$ m. Furthermore, the thickness of geotextile and geonet was also enlarged two times thicker than that of the physical model, i.e., thickness values of geonet and geotextile were 10 and 5 mm, respectively.

The results of the simulations are plotted in Fig. 3. Since the calculations were extracted from the double-sized model, the dimensions shown in Fig. 3 are presented in terms of ratios to the wall height H. Good agreement between the data from the physical tests and the corresponding simulations was obtained from the plots, proving that the relevant seepage responses, including water content and ground water level, were well captured using the established model in the Plaxis environment regardless of the size of the model.

The numerical experiment was carried out in two parts. In the first part, a series of numerical simulations were produced to investigate the individual effects of shape parameters W, H, L, and D on seepage responses, including the highest water level in the protected (ho), and the water saturation profile inside the protected zone. During the experiment, all the shape parameters, except the parameter being varied, were kept constant at $H = 2.0$ m, $W = 1.6$ m, $L = 2.0$ m, and $D = 0.8$ m. The simulations were conducted in three scenarios based on the soil types prescribed as native and backfill soils. The numerical simulations conducted in this part are summarized in Tables 2 and 3. It is noteworthy that the *S-S* scenario, which the native and backfill soils were placed by the sandy soil, rarely exists in field conditions. This scenario, however, was established for the sake of comparison. In total, 66 simulations were made, 22 for each scenario. The height of upstream water level H_w was kept constant at 2.0 m through 66 simulation cases. The model parameters imposed for the seepage characters of the sandy soil, lateritic soil, geotextile, and geonet were those reported by Chinkulkijniwat et al. (2017) and Bui Van et al. (2017) and are presented in Table 1. These model parameters (k, α, n, S_{res}, S_{sat}) including thickness of geotextile and geonet were kept constant throughout the first part of the numerical experiment.

The second part of the numerical experiment comprised 27 cases. In this part, a series of numerical simulations was

Table 1. Basic and relevant physical and hydraulic properties of studied sandy soil, geotextile, geonet (adapted from Chinkulkijniwat et al. 2017), and lateritic soil (adapted from Bui Van et al. 2017) utilized in this study

	Physical property								Hydraulic property and VG model parameter						
Material	γ (kN/m^3)	G_s (—)	PL (%)	LL (%)	Porosity (—)	Open size (mm)	Weight per area (kg/m^2)	Thickness (mm)	Permeability (m/s)	Transmissivity $\times 10^{-6}$ (m^2/s)	Permittivity (s^{-1})	α (m^{-1})	n (—)	S_{sat} (—)	S_{res} (—)
Soil material															
Sandy soil	15.0	2.74	—	—	—	—	—	—	1.97×10^{-4}	—	—	20	1.5	1.0	0.03
Lateritic soil	18.27	2.75	26	42	—	—	—	—	4.0×10^{-6}	—	—	0.8	1.4	1.0	0.2
Geosynthetic material															
Geotextiles	—	—	—	—	0.9	0.15	0.339	2.5	2.3×10^{-2} (0.37×10^{-2})[a]	57.9 (9.26)[b]	9.23 (1.48)[c]	20	2.5	0.8	0.03
Geonet	—	—	—	—	—	—	1.0	5.0	80×10^{-2}	0.004	160	600	40	1.0	0.0

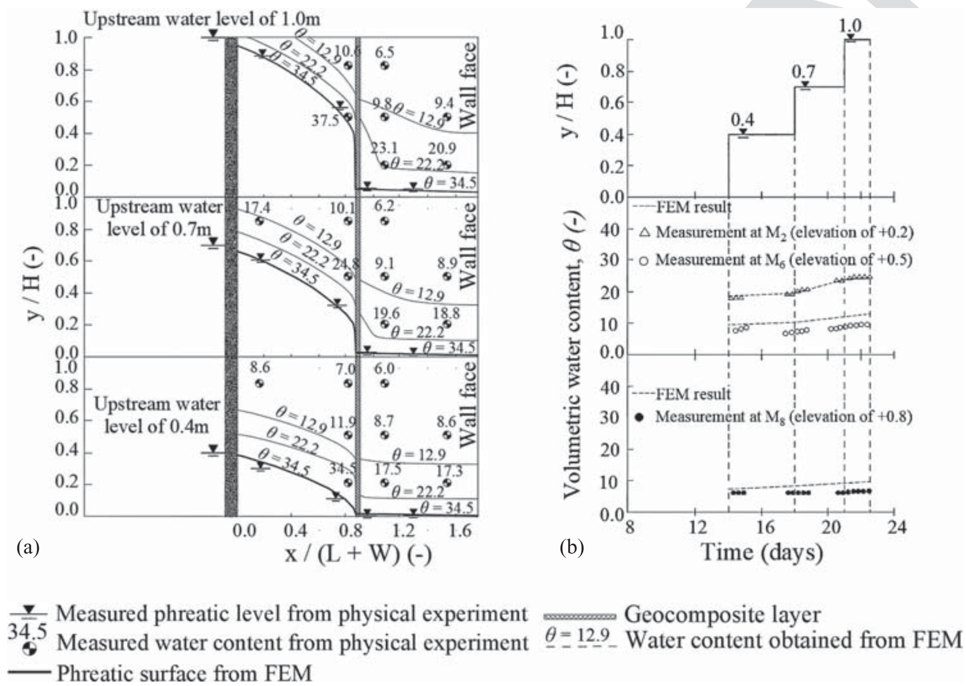

Fig. 3. (a) Water saturation profiles, phreatic level adopted from the physical model test reported in adapted from Chinkulkijniwat et al. (2017) and the corresponding calculations; and (b) time series plot of water content adopted from the physical model test report adapted from Chinkulkijniwat et al. (2017) and the corresponding calculations.

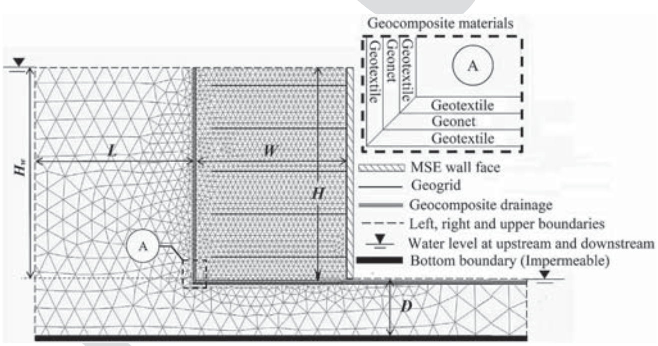

Fig. 4. Plaxis model of mesh discretization and the relevant shape parameters of the MSE wall with back drain using geocomposite.

produced to investigate the effects of geonet transmissivity (T_{net}) on seepage responses, including the highest water level in the protected (h_o), and the water saturation profile inside the protected zone. Geonet transmissivity was controlled by geonet thickness (t_{net}) and geonet permeability (k_{net}) through the following relationship:

$$T_{net} = k_{net} \times t_{net} \tag{4}$$

where T_{net} = geonet transmissivity (m^2/s); t_{net} = geonet thickness (m); and k_{net} = geonet permeability (m/s). In this experimental part, all the shape parameters were kept constant at $H = 2.0$ m, $W = 1.6$ m, $H_w = 2.0$ m, $L = 2.0$ m, and $D = 0.8$ m. The t_{net} was varied at 10, 15, and 20 mm, while the k_{net} was varied at 0.8, 0.08, and 0.008 m/s. The simulations were also conducted in three scenarios based on the soil types prescribed as native and backfill soils. Tables 4 and 5 summarize details of the second part of the numerical experiment.

A steady flow mode was selected to calculate the final groundwater states due to elevated upstream water. The groundwater states at steady state, including h_o and water saturation, extracted from the numerical experiment were used to analyze the influence of the studied parameters.

Influence of Shape Parameters

This section describes, via the location of the phreatic surface and the distribution of water saturation inside the protected zone, the influence of shape parameters W, H, D, and L. The location of the phreatic surface inside the protected zone was represented by its highest level (h_o), and the distribution of water saturation inside the protected zone was determined from the water saturation profile in the protected zone along a vertical section located at 0.8 m apart from the drainage interface.

Table 2. Three scenarios conducted in the shape parameter study

Scenario	Native soil	Backfill soil
S-S	Sandy soil	Sandy soil
L-L	Lateritic soil	Lateritic soil
L-S	Lateritic soil	Sandy soil

Note: The height of upstream water level (H_w) was kept constant at 2.0 m for all 66 simulations.

Table 3. Variation of shape parameters in the shape parameter study

Varied parameter	Definition	Referenced value	Varied values
W (m)	Protected zone width	1.6	2.0, 2.5
L (m)	Length from upstream water to the drainage face	2.0	0.5, 1.0, 3.0, 4.0, 5.0
H (m)	MSE wall height	2.0	2.5, 3.0, 3.5, 4.0, 4.5, 5.0
D (m)	Distance from the wall base to the impervious boundary	0.8	0.0, 0.2, 0.5, 1.0, 2.0, 3.0, 4.0, 5.0

Note: The height of upstream water level (H_w) was kept constant at 2.0 m for all 66 simulations.

Table 4. Three scenarios conducted in T_{net} study

Scenario	Native soil	Backfill soil
S-S	Sandy soil	Sandy soil
L-L	Lateritic soil	Lateritic soil
L-S	Lateritic soil	Sandy soil

Table 5. Variation of geonet thickness and geonet permeability in the T_{net} study

Varied parameter	Definition	Studied values
t_{net} (mm)	Geonet thickness	10, 15, 20
k_{net} (m/s)	Geonet permeability	0.8, 0.08, 0.008

Note: Geometry parameters are kept constant at $H(H_w) = 2.0$ m, $L = 2.0$ m, $D = 0.8$ m, $W = 1.6$ m.

Highest Water Level Inside Protected Zone (h_o)

For the sake of brevity and comparability, the variations of h_o for every shape parameter and every scenario were plotted together (Fig. 5). For the *S-S* scenario, the native soil was sandy soil which was different from *L-L* and *L-S* scenarios whose native soil was lateritic soil. The calculation results show that h_o in the *S-S* scenario was higher than that in *L-L* and *L-S* scenarios. In fact, the phreatic surfaces in every scenario before approaching the geocomposite were not much different (Fig. 6). The significant difference of phreatic surface took place only near the drainage interface.

It is known that flow across a boundary between two materials of different permeabilities might result in a reflection of the flow direction (as shown in Fig. 6), and the relationship between the reflected angles and the permeability of the materials is written as follows:

$$\frac{\tan \beta_1}{\tan \beta_2} = \frac{k_1}{k_2} \tag{5}$$

where β_1 = incident angle or angle of flow vectors in the native soil; β_2 = reflected angle or angle of flow vectors in the drainage material; k_1 = permeability of the native soil; and k_2 = permeability of drainage material.

Since the drainage material possessed very high permeability, the flow vectors in the drainage material directed almost vertical, i.e., β_2 was almost 90°. The flow vectors in the soil before approaching the drainage interface had to direct themselves such that the relationship between the incident angle (β_1) and the reflected angle (β_2) followed Eq. (5). For a given permeability of drainage material, the high permeability native soil yielded the higher incident angle than the low permeability native soil did. Accordingly, near the drainage interface, the phreatic surface in *L-L* and *L-S* scenarios dropped below the phreatic surface in the *S-S* scenario.

Fig. 5 also shows that the h_o band in the *L-L* scenario was higher than the band in the *L-S* scenario, indicating a higher mean phreatic surface in the *L-L* scenario than that in the *L-S* scenario.

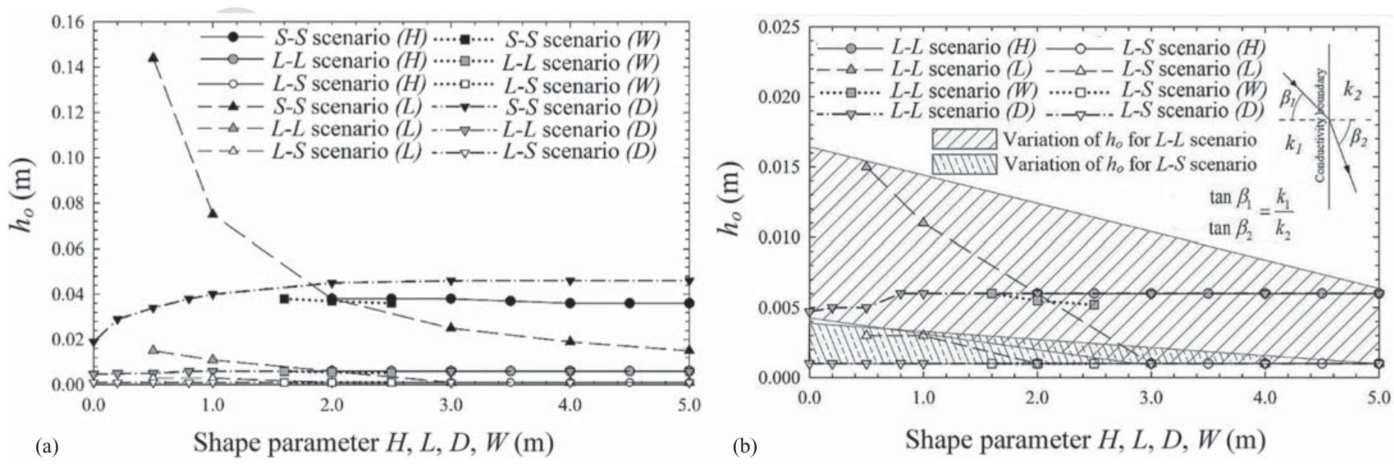

Fig. 5. (a) Variation of h_o subjected to change in all shape parameters for *S-S*, *L-L*, and *L-S* scenarios; and (b) variation of h_o subjected to change in all shape parameters for *L-L* and *L-S* scenarios.

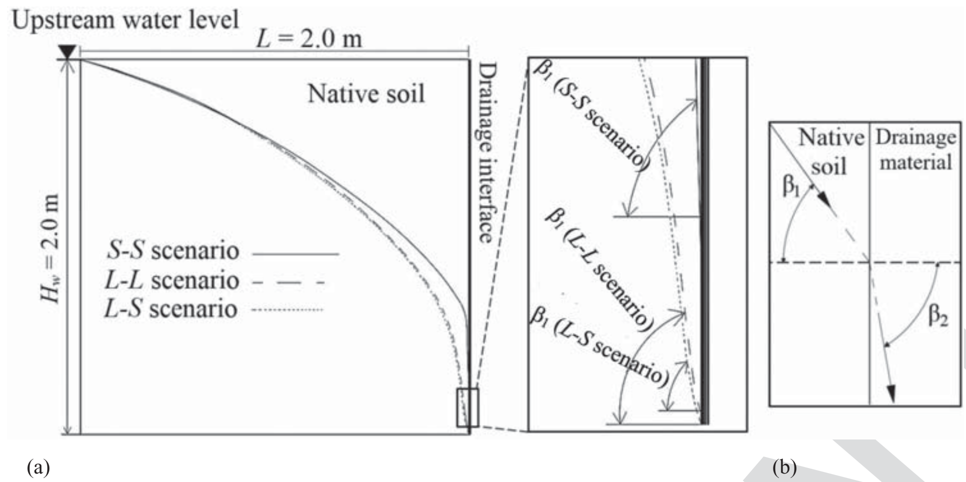

Fig. 6. (a) Phreatic surface approaching drain interface; and (b) reflection of flow directed from native soil to drain material.

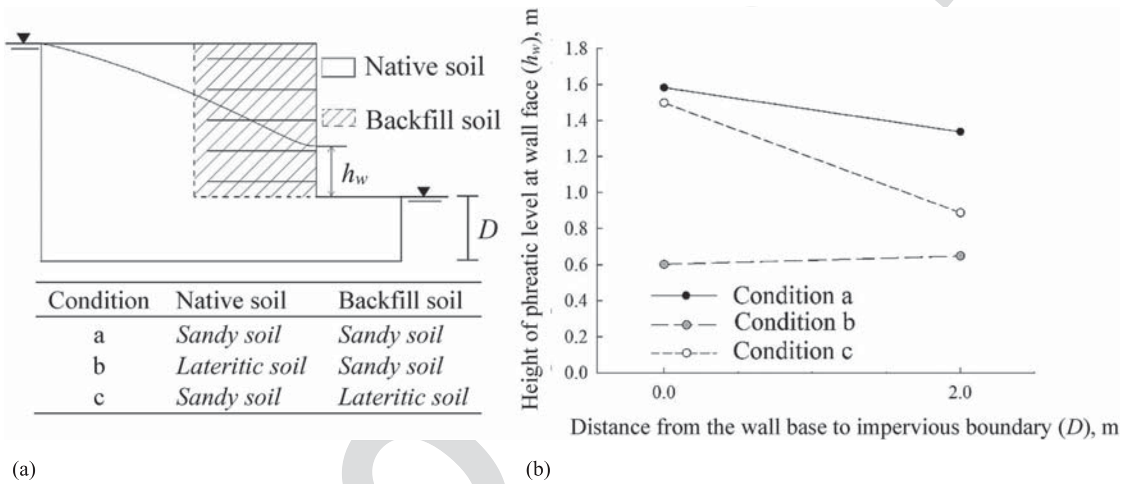

Fig. 7. (a) Setup of Conditions a, b, and c for modeling of the MSE wall without back drain installation; and (b) variation of h_w with D for Conditions a, b, and c.

This finding is similar to that reported in Bui Van et al. (2017). They argued that soil in the protected zone was more permeable in the *L-S* scenario than in the *L-L* scenario; therefore, the flow path reflection resulted in the lower phreatic surface in the protected zone for the *L-S* scenario than that for the *L-L* scenario.

Dimensions of the Protected Zone

The dimensions of the protected zone comprised the protected zone width (W) and the wall height (H). It is widely accepted that these shape parameters play important roles in the mechanical responses and hence internal and external stabilities of an MSE wall (Roy and Singh 2008; Studlein et al. 2012; Kibria et al. 2014). However, the effect of these shape parameters on the seepage responses in an MSE wall is yet to be investigated. In this study, since the protected zone was encapsulated by the geocomposite, W and H were also the length of geocomposite at the bottom and the backside of the protected zone, respectively. W was varied from 1.6 to 2.5 m. Based on the H value of 2.0 m, the W/H ratio in this study ranges from 0.8 to 1.25, which is about the practical recommendation of 0.8 to more than 1.1 (Berg et al. 2009). Keeping horizontal distance from upstream to downstream water sources constant at 5.0 m, h_o negligibly drops with W (Fig. 5). As for the influence of the wall height H on h_o, since this shape parameter has no effect on flow geometry, the value of h_o did not change with H, as indicated in Fig. 5.

Distance from the Wall Base to the Impervious Boundary (D)

Theoretically the distance from the base of an MSE wall to the impervious layer beneath, identified as the shape parameter D, affects the discharge of water flowing beneath the wall to the downstream side. In a study of groundwater flow through a sheet pile barrier, Xu et al. (2014) reported 3D numerical experiments that indicated the downstream water level decreased at greater insertion depth ratios: i.e., a ratio between penetration depth and distance from the tip of the pile to the impervious layer. In MSE walls without a back drain, an influence of D distance depends on the combination of soil types in the flow domain. Fig. 7 presents the influence of D distance in three conditions of the MSE wall without back drain installation, including (a) the backfill and the native soils were identical; (b) the backfill soil was sandy soil and the native soil was lateritic soil; and (c) the backfill soil was lateritic soil and the native soil was sandy soil. It is noteworthy that the last condition rarely exists in the real condition since it is no sense to use lateritic soil as backfill material if sandy is available. However, this study shows three different conditions, including the rarely exist condition (c), for the sake of comparison and understanding the flow behavior.

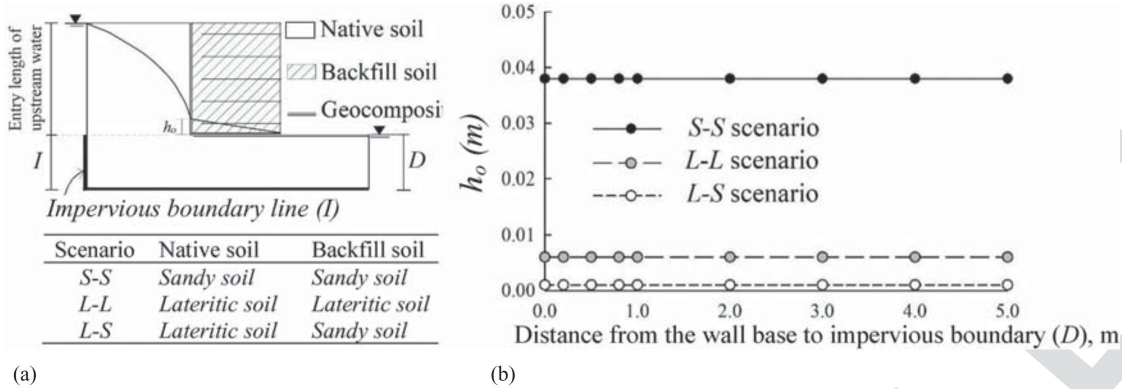

Fig. 8. (a) Setup of the extra numerical experiment to model MSE wall with back drain installation keeping the entry length of upstream water unchanged; and (b) variation of h_o with D.

For Condition (a), whose backfill and the native soils were identical, the greater D distance resulted in a lower phreatic level due to the existence of a larger flow channel beneath the protected zone. For Conditions (b) and (c), whose backfill and the native soils were different, the type of backfill soil played role in the flow behaviors. In Condition (b), whose backfill material was the sandy soil and the native soil was lateritic soil, the water flow tended to direct to the sandy soil as it possessed high permeability. For the larger D distance, there was the wider area to allow the water flow into the concerned domain. Since the water flow tended to direct to the sandy soil which was placed as backfill soil, enlarging D distance would result in a higher phreatic level. In Condition (c), the lateritic soil was placed as backfill soil and the native soil was sandy soil. Enlarging D distance resulted in the drop of phreatic level since the sandy soil which located below the MSE wall could accept more amount of water flow.

For an MSE wall with geocomposite back drain installation, enlarging D distance resulted in little rise of h_o level as shown in Fig. 5. Variation of h_o with D distance was found only within the limit range of D from 0.0 to 2.0 m. Increment of D beyond 2.0 m did not change the h_o level. It is noteworthy that the cases with D of 0.0 m were conducted to simulate impervious foundation at the wall base. However, it is yet to be clarified whether the contribution to this increment of h_o is due to the thickness of the foundation soil or the area of water contribution on the upstream side.

The extra numerical experiment was conducted in the MSE wall with the back drain installation model. In this model, the vertical impervious boundary of length I was prescribed at the bottom corner of the upstream side, as shown in Fig. 8. In this experiment enlarging the distance D was incorporated with extending the length of vertical impervious boundary line (I) such that the entry length of the upstream water [Fig. 8(a)] keeps unchanged at 2.0 m. Fig. 8(b) presents variation of h_o with D distance when the entry length of upstream water was kept constant. The h_o level did not change with D for all scenarios implying that the increment of h_o with D found in Fig. 5 was solely contributed by the entry length of the upstream water.

One must be aware that the geonet transmissivity, which is a product of geonet permeability ($k_{\text{net}} = 0.8$ m/s) and geonet thickness ($t_{\text{net}} = 10$ mm), assigned in this study is very high (0.008 m^2/s). In the field condition, reduction of geonet- and geotextile transmissivities might be encountered by various factors, including creep, mineral/biological clogging, geocomposite intrusion, damage on implementation, discontinuity at the connection, and so on. The conclusion drawn in this study is valid if the geocomposite does not exceed its drainage capacity.

Length from Upstream Water to the Drainage Face (*L*)

There is no doubt that the longer the distance from the upstream water to the drainage face (L), the more the hydraulic head falls and with it the phreatic level h_o at the downstream exit. Fig. 5(a) shows the variability of h_o with shape parameter L. When L was small, h_o fell very fast with increments of L but the rate of fall decreased when L was greater. In the *S-S* scenario, the magnitude of h_o approached asymptote when the shape parameter L was greater than 4.0 m, i.e., 200% of the wall height. This behavior implies that the influence of shape parameter L was eliminated if L was large enough. On the other hand, the phreatic height in the protected zone could be as high as 10% of the wall height when L was shorter than one-fourth of the wall height. When MSE walls are installed in mountainous areas, the distance from the upstream water source to the protected zone can be very short. Accordingly, engineers must pay close attention to the potential phreatic levels in the protected zone of an MSE wall in mountainous terrain.

Water Saturation Profile in the Protected Zone

The distribution of water saturation inside the protected zone was determined from the water saturation profile along the vertical line located at 0.8 m apart from the drainage interface. In general, the water saturation profile in a given soil is governed by the shape of the WRC and the phreatic level in the corresponding soil. Consequently, water saturation profiles in the protected zone were plotted according to the type of soil used as backfill material. Water saturation profiles for *S-S* and *L-S* scenarios are presented in Fig. 9(a) and profiles for the *L-L* scenario in Fig. 9(b). The profiles were plotted along a vertical direction, and they were plotted from the wall base to the top of the wall. In other words, the saturation profiles were plotted to equal height of the wall height (H). Since the wall height was kept constant at 2.0 m when modeling the influence of the shape parameters W, L, and D, the profiles for these shape parameters were generated from the elevation of 0.0 m at the wall base to the elevation of 2.0 m at the top of the wall [Figs. 9(a and b)]. For the shape parameter H, the height of the wall was varied from 2.0 to 5.0 m. The profiles must be extended equal to the height of the wall and plotted separately in Fig. 9(c).

In *S-S* and *L-S* scenarios, a high level of water saturation was found only near the wall base. The level dropped very fast with distance from the wall base and water saturation was lower than 50% at a height of 0.2 m from the wall base. The water saturation curve approached asymptote at the middle height of the wall. In the *L-L* scenario, water saturation dropped so slowly that it was greater than 80% over the entire height of the wall. The influences of the studied shape parameters on the water saturation profile are also presented

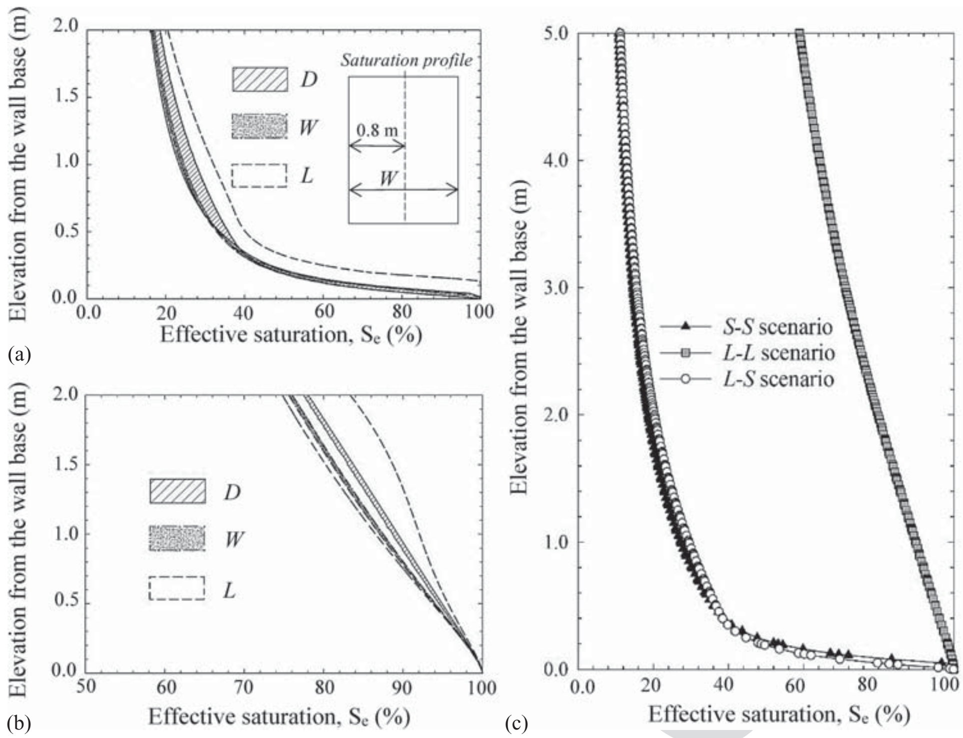

Fig. 9. (a) Water saturation profile subjected to variation of *D*, *W*, *L* shape parameter in *S-S* and *L-S* scenarios; (b) water saturation profile subjected to variation of *D*, *W*, *L* shape parameter in *L-L* scenario; and (c) water saturation profile for *H* shape parameter in 3 scenarios as *S-S*, *L-L* and *L-S*.

in Fig. 9. This figure combines the plots of all assigned values of every shape parameter and presents the plots as the boundaries of the profiles of each shape parameter. Wider boundaries indicate a greater influence of the corresponding shape parameter on the water saturation profile. As shown by the boundary plots in Fig. 9, the influence of all shape parameters on the water saturation profile is in accordance with the influence on h_o. The boundary width of water saturation profiles for shape parameter *L* is larger than it is for the other shape parameters. The water saturation profiles for shape parameter *H* are plotted as three single lines, one line for each scenario. There is little deviation between the water saturation profiles for *S-S* and *L-S* scenarios, in which the backfill soil was identical. This similarity indicates that the water saturation profile was mainly governed by the WRC of the corresponding soil.

Geocomposite Drain Properties

The transmissivity of the geonet (T_{net}) is widely accepted as a crucial property for drainage purposes (Gallichand et al. 1992; Clement et al. 1996; Koerner et al. 2005; Giroud et al. 2000; Bourgès-Gastaud et al. 2013; Yarahmadi et al. 2017). In Plaxis, the magnitude of T_{net} must be prescribed through the geonet thickness (t_{net}) and its permeability (k_{net}). A series of numerical simulations were produced to investigate the individual effects of t_{net} and k_{net} on seepage responses, including the highest water level in the protected zone (h_o), and the water saturation profile inside the protected zone. The t_{net} and k_{net} were varied at 10 and 20 mm and 0.8 and 0.008 m/s, respectively (Table 5).

Fig. 10 presents the variation of water saturation profile with t_{net} for three studied scenarios having k_{net} of 0.8 m/sec. The profiles were plotted along a vertical section at 0.8 m apart from the drainage interface inside the protected zone. In general, varying t_{net} had very little effect on the water saturation profile. The water

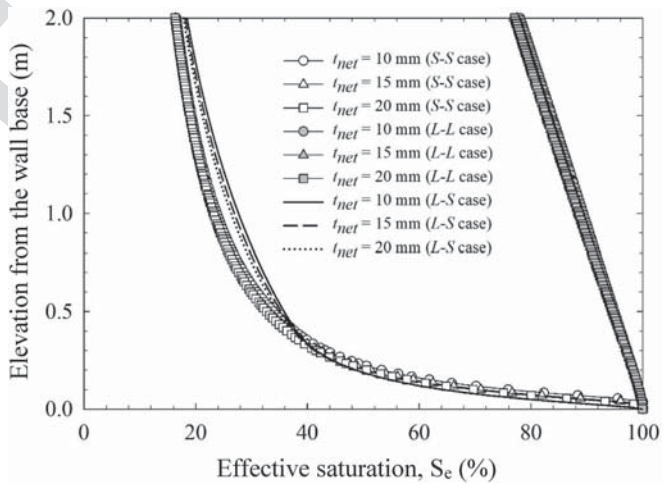

Fig. 10. Water saturation profile subjected to the variation of geonet thickness (t_{net}) in *S-S*, *L-L*, and *L-S* scenarios.

saturation profile in the protected zone mainly depended on the soil type prescribed. Since the soil type in the protected zone in *S-S* and *L-S* scenarios was sandy soil, and in the *L-L* scenario, lateritic soil, the water saturation profiles of *S-S* and *L-S* scenarios differed significantly from the profiles of the *L-L* scenario. Furthermore, Fig. 10 also shows little difference in the water saturation profiles of *S-S* and *L-S* scenarios. In the *S-S* scenario, water saturation in the lower part of the protected zone was greater than in the *L-S* scenario because the phreatic level inside the protected zone in the *S-S* scenario was higher than in the *L-S* scenario [Fig. 5(a)]. However, in the upper part of the protected zone, water saturation was higher in the *L-S* scenario than in the *S-S* scenario. Figs. 11(a and b) present suction profiles over the domains in question for *S-S* and *L-S* scenarios, respectively. The variation of suction with

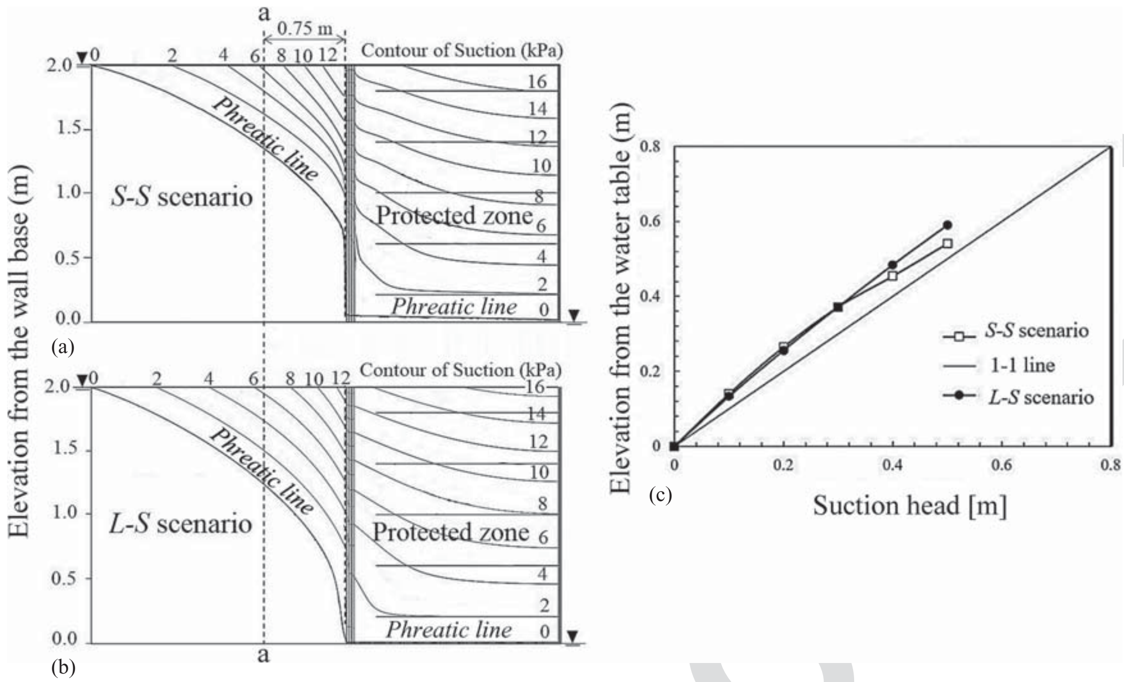

Fig. 11. (a) Suction profiles for the *S-S* scenario; (b) suction profiles for the *L-S* scenario; and (c) variation of suction with elevation above water table along vertical section *a-a* located at 0.75 m right apart from the drainage interface.

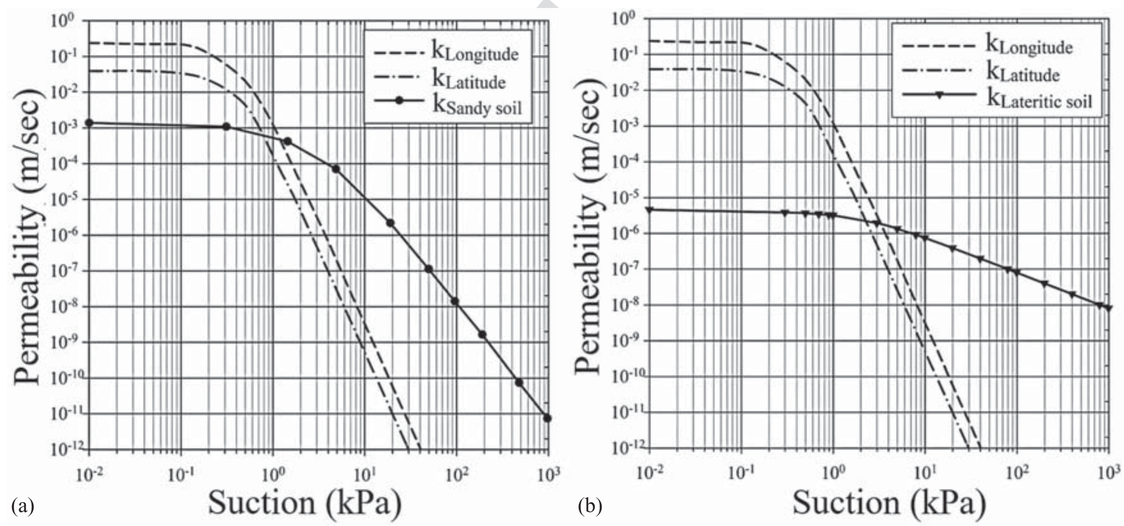

Fig. 12. (a) *k*-Functions of the geotextile and native soil for the *S-S* scenario; and (b) *k*-functions of the geotextile and native soil for the *L-S* scenario.

elevation above the water table along a vertical section *a-a* located at 0.75 m right apart from the drainage interface is shown in Fig. 11(c). Since the water flow directed inclined downward to the downstream side, the variation of suction with elevation above water table deviated from 1:1 line to the left (Bear 1972). Fig. 12 plots the *k*-function curves of the geotextile and the native soil. The suction at the place where water started penetrating the geocomposite in both scenarios was read from the point where plots of *k*-functions intersected. The suction values at the intersection of *k*-functions are about 1 and 3 kPa in *S-S* and *L-S* scenarios, respectively. Water saturation in the upper part of the protected zone was higher in the *L-S* scenario than in the *S-S* scenario because, in the *L-S* scenario, water started to penetrate the geocomposite at a higher elevation [Figs. 12(a and b)].

Fig. 13 presents the effects of t_{net} and k_{net} on h_o in the three studied scenarios. Increasing t_{net} and/or k_{net} produced a fall in h_o due to the increased capacity of the drainage channel. The h_o axis was plotted in a log scale for the sake of ease comparison. For each k_{net}, the ratio of h_o for the lowest t_{net} to h_o for the highest t_{net} value is indicated as the number appeared on the corresponding line. The drop of the h_o ratio with increasing t_{net} is greater for the higher k_{net}, which means that the reduction of h_o by enlarging geonet thickness is more effective in the higher geonet permeability. These data sets were further employed to investigate the relationship between h_o and geonet transmissivity (T_{net}), as plotted in Fig. 14.

Fig. 14 shows the variation of h_o against geonet transmissivity (T_{net}) in the semi-log scale for the three studied scenarios. A linear

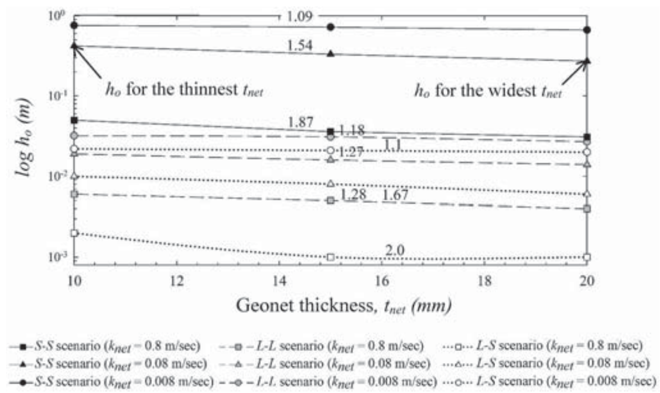

Fig. 13. Variation of h_o subjected to the effect geonet thickness (t_{net}) and geonet permeability in *S-S*, *L-L*, *L-S* scenarios. (The number appeared on the corresponding line is ratio of h_o for the lowest t_{net} to h_o for the highest t_{net}.)

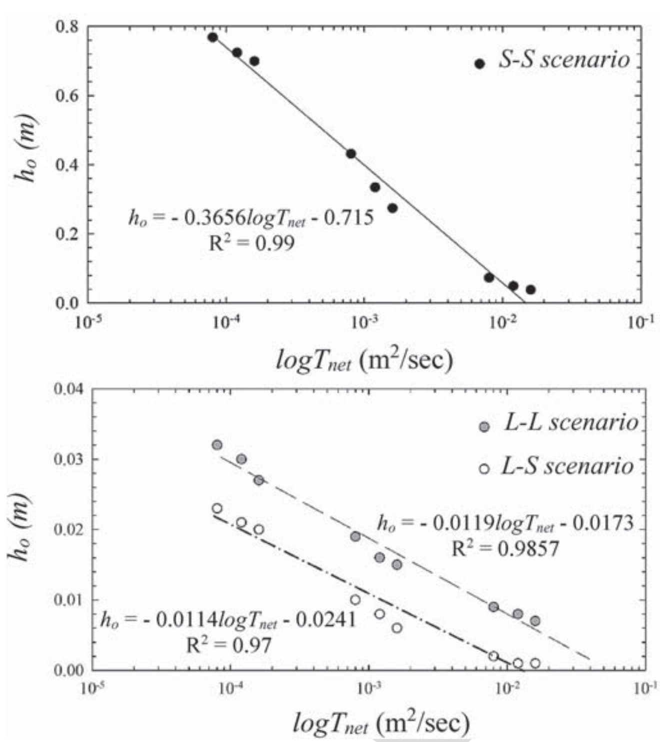

Fig. 14. Linear relationship between h_o and log T_{net} for all 27 cases conducted in the second part of the numerical experiment.

relationship existed between h_o and ln T_{net} that was represented with a coefficient of determination (r^2) greater than 0.96. The gradients of the linear plots were equal to 0.36 in the *S-S* scenario and 0.01 in *L-L* and *L-S* scenarios. The identical gradients in *L-L* and *L-S* scenarios indicate that the fall in h_o with increments of ln T_{net} was mainly governed by the soil type on the upstream side. Since the gradient in the *S-S* scenario was 36 times steeper than in *L-L* and *L-S* scenarios and the permeability coefficient of the upstream soil in the *S-S* scenario was 49 times the permeability coefficient in *L-L* and *L-S* scenarios, taking into account the very wide range of the permeability coefficients ($1.0 - 10^{-12}$ m/s), the gradient ratio of 36:1 is not very different from the permeability coefficient ratio of 49:1. The conclusion was drawn that a significant correlation existed between the rate of fall in h_o with ln T_{net} and the permeability coefficient of the upstream soil.

Conclusions

This article investigated the influence of relevant shape parameters on seepage responses, including the highest water level in the protected (h_o) and the water saturation in the protected zone, in an MSE wall with a geocomposite back drain. Other than the relevant shape parameters, the influence of geonet transmissivity, which is a main component of geocomposite drainage systems, was also investigated. The following conclusions were drawn from this study.

- Where the distance from the upstream water to the drainage face (L) is short, this shape parameter (L) plays a significant role in the seepage responses in the MSE wall. Accordingly, involved engineers must pay close attention to the phreatic level in the protected zone when dealing with an MSE wall in a mountainous area, where the distance from upstream water to the drainage face might be very short (Fig. 5).
- The height of the wall (H) and the width of protected zone (W) play no to negligible role in the magnitude of h_o. However, the vertical distance from the wall base to the impervious boundary (D) also plays no role in the magnitude of h_o whenever the contribution upstream water source does not change (Fig. 8). This conclusion is based on an assumption that the geocomposite does not exceed its drainage capacity.
- Water saturation in the protected zone mainly depended on the water retention curve of the soil used as fill materials (Figs. 9 and 10).
- Although distribution of water saturation in the protected zone mainly depends on the properties of backfill material, the k-function of the soil at the upstream side might play little role in the water distribution in the protected zone particularly at the upper elevation. This conclusion is based on k-function plots of upstream soils and geotextile (Figs. 10–12).
- The permeability of the upstream soil is important properties contributing to the h_o level. The difference between the permeability of the drainage material and that of the upstream soil governs the h_o value (Fig. 6). Furthermore, the permeability coefficient of the soil on the upstream side governs the rate at which h_o falls with increments of geonet transmissivity. The greater the permeability coefficient of the upstream soil, the faster h_o falls with geonet transmissivity (Fig. 14).

Data Availability Statement

All data and models generated or used during the study are available from the corresponding author by request. The following are the list of data and models used in this study.

1. MSE wall models in the Plaxis environment having various wall dimensions with and without back drain installation.
2. MSE wall with back drain installation models in the Plaxis environment having various geonet thickness (t_{net}) and geonet permeability (k_{net}).
3. All calculation results mentioned in this study include the following:
   - Variation of h_o subjected to the change in all shape parameters, geonet thickness (t_{net}), and geonet permeability (k_{net}) for *S-S, L-L,* and *L-S* scenarios,
   - Variation of water saturation profile subjected to the change in all shape parameters, geonet thickness (t_{net}), and geonet permeability (k_{net}) for *S-S*, *L-L,* and *L-S* scenarios.

Acknowledgments

This research was financially supported by the Thailand Research Fund (Grant No. RSA6080055) and the SUT Research and Development Fund.

Notation

The following symbols are used in this paper:

D = distance from the wall base to the impervious boundary (m);
G_s = specific gravity (—);
H = MSE wall height (m);
H_W = height of upstream water level (m);
h = total head (m);
h_o = highest water level inside protected zone;
h_p = matric suction head (m);
h_w = height of phreatic level at wall face (m);
I = length of vertical impervious boundary line (m);
k = coefficient of permeability (m/s);
k_{Latitude} = coefficient of permeability of geotextile in the x-directions (m/s);
$k_{\text{Longtitude}}$ = coefficient of permeability of geotextile in the y-directions (m/s);
k_{net} = geonet permeability (m/s);
k_r = coefficient of relative permeability (—);
k_x = coefficients of permeability in the x-directions (m/s);
k_y = coefficients of permeability in the y-directions (m/s);
L = length from upstream water to the drainage face (m);
m = VG model parameter (—);
n = VG model parameter (—);
S = degree of saturation (—);
S_e = effective degree of saturation (—);
S_{res} = residual saturation (—);
S_{sat} = saturated saturation (—);
T_{net} = geonet transmissivity (m^2/s);
t = time (s);
t_{net} = geonet thickness (m);
W = protected zone width (m);
α = VG model parameter (m^{-1});
β_1 = incident angle or angle (deg.);
β_2 = reflected angle (deg.);
γ = unit weight (kN/m^3);
θ = volumetric water content (—);
θ_{res} = residual volumetric water content (—); and
θ_{sat} = saturated volumetric water content (—).

References

Albino, U. D. R., F. H. M. Portelinha, J. G. Zornberg, and M. M. Futai. 2019. "Numerical simulation of infiltration into the fill of a wall reinforced with nonwoven geotextiles." *Comput. Geotech.* 108: 27–39. https://doi.org/10.1016/j.compgeo.2018.12.006.

Bear, J. 1972. *Dynamics of fluids in porous media*. New York: Dover.

Berg, R., B. R. Christopher, and N. Samtani. 2009. *Design of mechanically stabilized earth walls and reinforced soil slopes—Vol. 1*. Rep. No. FHWA-NHI-10-024. Washington, DC: Federal Highway Administration.

Bourgès-Gastaud, S., E. Blond, and N. Touze-Foltz. 2013. "Multiscale transmissivity study of drain-tube planar geocomposites: Effect of experimental device on test representativeness." *Geosynth. Int.* 20 (3): 119–128. https://doi.org/10.1680/gein.13.00006.

Bui Van, D., A. Chinkulkijniwat, S. Horpibulsuk, S. Yubonchit, I. Limrat, A. Arulrajah, and C. Jothityangkoon. 2017. "Steady flow in mechanically stabilised earth walls using marginal soils with geocomposites." *Geosynth. Int.* 24 (6): 590–606. https://doi.org/10.1680/jgein.17.00026.

Chinkulkijniwat, A., S. Horpibulsuk, D. Bui Van, A. Udomchai, R. Goodary, and A. Arulrajah. 2017. "Influential factors affecting drainage design considerations for mechanical stabilised earth walls using geocomposite." *Geosynth. Int.* 24 (3): 224–241.

Christopher, B., J. Zornberg, and J. Mitchell. 1998. "Design guidance for reinforced soil structures with marginal soil backfills." In *Proc., 6th Int. Conf. on Geosynthetics*, 797–804.

Clement, T. P., W. R. Wise, F. J. Molz, and M. Wen. 1996. "A comparison of modeling approaches for steady-state unconfined flow." *J. Hydrol.* 181 (1–4): 189–209. https://doi.org/10.1016/0022-1694(95)02904-4.

Dickinson, S., R. W. I. Brachman, and R. K. Rowe. 2010. "Thickness and hydraulic performance of geosynthetic clay liners overlying a geonet." *J. Geotech. Geoenviron. Eng.* 136 (4): 552–561. https://doi.org/10.1061/(ASCE)GT.1943-5606.0000247.

Escario, V., and J. Sáez. 1986. "The shear strength of partly saturated soils." *Géotechnique* 36 (3): 453–456. https://doi.org/10.1680/geot.1986.36.3.453.

Fredlund, D. G., N. R. Morgenstern, and R. A. Widger. 1978. "The shear strength of unsaturated soils." *Can. Geotech. J.* 15 (3): 313–321. https://doi.org/10.1139/t78-029.

Gallichand, J., D. Marcotte, and S. O. Prasher. 1992. "Including uncertainty of hydraulic conductivity into drainage design." *J. Irrig. Drain. Eng.* 118 (5): 744–756. https://doi.org/10.1061/(ASCE)0733-9437(1992)118:5(744).

Giroud, J. P., and E. Kavazanjian. 2014. "Degree of turbulence of flow in geosynthetic and granular drains." *J. Geotech. Geoenviron. Eng.* 140 (5): 06014001. https://doi.org/10.1061/(ASCE)GT.1943-5606.0001086.

Giroud, J. P., J. G. Zornberg, and A. Zhao. 2000. "Hydraulic design of geosynthetic and granular liquid collection layers." *Geosynth. Int.* 7 (4–6): 285–380. https://doi.org/10.1680/gein.7.0176.

Iryo, T., and R. K. Rowe. 2004. "Numerical study of infiltration into a soil–geotextile column." *Geosynth. Int.* 11 (5): 377–389. https://doi.org/10.1680/gein.2004.11.5.377.

Kibria, G., M. S. Hossain, and M. S. Khan. 2014. "Influence of soil reinforcement on horizontal displacement of MSE wall." *Int. J. Geomech.* 14 (1): 130–141. https://doi.org/10.1061/(ASCE)GM.1943-5622.0000297.

Koerner, R. M., and G. R. Koerner. 2011. "The importance of drainage control for geosynthetic reinforced mechanically stabilized earth walls." *J. Geoeng.* 6 (1): 3–13.

Koerner, R. M., and G. R. Koerner. 2013. "A data base, statistics and recommendations regarding 171 failed geosynthetic reinforced mechanically stabilized earth (MSE) walls." *Geotext. Geomembr.* 40: 20–27. https://doi.org/10.1016/j.geotexmem.2013.06.001.

Koerner, R. M., and G. R. Koerner. 2015. "Lessons learned from geotextile filter failures under challenging field conditions." *Geotext. Geomembr.* 43 (3): 272–281. https://doi.org/10.1016/j.geotexmem.2015.01.004.

Koerner, R. M., and G. R. Koerner. 2018. "An extended data base and recommendations regarding 320 failed geosynthetic reinforced mechanically stabilized earth (MSE) walls." *Geotext. Geomembr.* 46 (6): 904–912. https://doi.org/10.1016/j.geotexmem.2018.07.013.

Koerner, R. M., T.-Y. Soong, G. R. Koerner. 2005. "Back drainage design and geocomposite drainage materials." In *Proc., GRI-19 Conf.*, 51–86.

McKean, J., and K. Inouye. 2001. "Field evaluation of the long-term performance of geocomposite sheet drains." *Geotext. Geomembr.* 19 (4): 213–234. https://doi.org/10.1016/S0266-1144(01)00007-3.

Mitchell, J. K., and J. G. Zornberg. 1995. "Reinforced soil structures with poorly draining backfills—Part II: Case histories and applications." *Geosynth. Int.* 2 (1): 265–307. https://doi.org/10.1680/gein.2.0011.

Mualem, Y. 1976. "A new model for predicting the hydraulic conductivity of unsaturated porous media." *Water Resour. Res.* 12 (3): 513–522. https://doi.org/10.1029/WR012i003p00513.

Robinson, J. D., F. Vahedifard, and A. AghaKouchak. 2017. "Rainfall-triggered slope instabilities under a changing climate: Comparative study using historical and projected precipitation extremes." *Can. Geotech. J.* 54 (1): 117–127. https://doi.org/10.1139/cgj-2015-0602.

Roy, D., and R. Singh. 2008. "Mechanically stabilized earth wall failure at two soft and sensitive soil sites." *J. Perform. Constr. Facil* 22 (6): 373–380. https://doi.org/10.1061/(ASCE)0887-3828(2008)22:6(373).

Saeedpanah, I., E. Jabbari, and M. A. Shayanfar. 2011. "Numerical simulation of ground water flow via a new approach to the local radial point interpolation meshless method." *Int. J. Comput. Fluid Dyn.* 25 (1): 17–30. https://doi.org/10.1080/10618562.2010.545772.

Stuedlein, A. W., T. M. Allen, R. D. Holtz, and B. R. Christopher. 2012. "Assessment of reinforcement strains in very tall mechanically stabilized earth walls." *J. Geotech. Geoenviron. Eng.* 138 (3): 345–356. https://doi.org/10.1061/(ASCE)GT.1943-5606.0000586.

Thuo, J. N., K. H. Yang, and C. C. Huang. 2015. "Infiltration into unsaturated reinforced slopes with nonwoven geotextile drains sandwiched in sand layers." *Geosynth. Int.* 22 (6): 457–474. https://doi.org/10.1680/jgein.15.00026.

Vahedifard, F., F. S. Tehrani, V. Galavi, E. Ragno, and A. AghaKouchak. 2017. "Resilience of MSE walls with marginal backfill under a changing climate: Quantitative assessment for extreme precipitation events." *J. Geotech. Geoenviron. Eng.* 143 (9): 04017056. https://doi.org/10.1061/(ASCE)GT.1943-5606.0001743.

van Genuchten, M. T. 1980. "A closed-form equation for predicting the hydraulic conductivity of unsaturated soils." *Soil Sci. Soc. Am. J.* 44 (5): 892–898. https://doi.org/10.2136/sssaj1980.03615995004400050002x.

Xu, Y.-S., S.-L. Shen, L. Ma, W.-J. Sun, and Z.-Y. Yin. 2014. "Evaluation of the blocking effect of retaining walls on groundwater seepage in aquifers with different insertion depths." *Eng. Geol.* 183: 254–264. https://doi.org/10.1016/j.enggeo.2014.08.023.

Yarahmadi, N., I. Gratchev, D. S. Jeng, and D. Gibbs. 2017. "Effect of thickness reduction on hydraulic transmissivity of geonets used in leachate collection systems in landfills." In *Proc., 19th Southeast Asian Geotechnical Conf. and 2nd AGSSEA Conf.*

Yoo, C., and H.-Y. Jung. 2006. "Case history of geosynthetic reinforced segmental retaining wall failure." *J. Geotech. Geoenviron. Eng.* 132 (12): 1538–1548. https://doi.org/10.1061/(ASCE)1090-0241(2006)132:12(1538).

Zhang, C., X. Chen, and W. Fan. 2016. "Overturning stability of a rigid retaining wall for foundation pits in unsaturated soils." *Int. J. Geomech.* 16 (4): 06015013. https://doi.org/10.1061/(ASCE)GM.1943-5622.0000613.

Zornberg, J. G., R. J. Barrows, B. R. Christopher, and J. K. Mitchell. 1995. "Constructing a geotextile-reinforced slope." *Geotech. Fabr. Rep.* 13 (7): 26–28.

Zornberg, J. G., and J. K. Mitchell. 1994. "Reinforced soil structures with poorly draining backfills. Part I: Reinforcement interactions and functions." *Geosynth. Int.* 1 (2): 103–147. https://doi.org/10.1680/gein.1.0006.

Queries

1. Please provide the ASCE Membership Grades for all authors who are members.

2. "Lafleur et al. (2000)" is cited in the sentence beginning "The wetting phase WRC…"; however, this reference does not appear to be included in the reference list. Please provide full details for this reference and add this reference to the reference list or remove this citation from the text.

3. Please include references details for the specification ASTM D6836-02 in the reference list.

4. "Kool and Parker (1987)" is cited in the sentence beginning "After getting the best-fit…"; however, this reference does not appear to be included in the reference list. Please provide full details for this reference and add this reference to the reference list or remove this citation from the text.

5. Please provide the name and location of the publisher of the proceedings for the reference "Christopher et al. (1998)." If there is no publisher, please provide the name and location of the sponsor of the conference. For sponsors that are virtual groups (without a physical location), include the conference location instead of sponsor location and the URL for the group's website.

6. Please provide the name and location of the publisher of the proceedings for the reference "Koerner et al. (2005)." If there is no publisher, please provide the name and location of the sponsor of the conference. For sponsors that are virtual groups (without a physical location), include the conference location instead of sponsor location and the URL for the group's website.

7. Reference "Mitchell and Zornberg (1995)" is listed in the reference list but not cited in the text. Please cite in the text, else delete from the list.

8. Please provide the name and location of the publisher of the proceedings for the reference "Yarahmadi et al. (2017)." If there is no publisher, please provide the name and location of the sponsor of the conference. For sponsors that are virtual groups (without a physical location), include the conference location instead of sponsor location and the URL for the group's website.

9. Please provide the significance of the indicators (a,b,c) in Table 1.